Biomimetic Morphogenesis and Structure of Calcite Statoliths (Otoconia): An Approach towards Deeper Understanding of a Bio-Sensor and its Function

Ya-Xi Huang, Jana Buder, Horst Borrmann, Raul Cardoso-Gil, Wilder Carrillo-Cabrera, Yurii Prots, Paul Simon, and Rüdiger Kniep

Introduction

The inner ear of vertebrates contains a complex arrangement of enclosed sacs and channels where the senses for balance and hearing are located. Parts of these sensory systems are called maculae. These organs act as gravity receptors by responding to linear accelerations [1]. The sensory transduction depends on the inertial mass of a calcium carbonate biomineral (so-called statolith). It consists of aragonite or, sometimes even of vaterite (so-called otoliths) [2,3] in case of fish and amphibians, while in reptiles, birds and mammals the calcite modification (so-called otoconia) is found [1]. A major difference between otoliths (ear stones; mm-sized) [4] and otoconia (ear dust; µm-sized) [5] is that the otoliths display a daily growth pattern, whereas adult otoconia are essentially inert and undergo only little changes with time. Furthermore, the otoconia are made up of thousands of tiny biomineral particles, each showing a barrel-shaped habit with triplanar faceted ends [5-7]. Mammalian otoconia (SEM-image) are presented in Fig. 1 (top); a schematic of the gravity receptor organ (macula) is depicted at the bottom of Fig. 1. The peculiar shape of the otoconia as well as their inner structure and the resulting biofunctionality are far from being fully understood up to now. The same is true for the shape development (morphogenesis). The present report contributes to these essential questions by a close biomimetic approach and describes the development of a complex composite architecture resembling all the structural details which are known from natural otoconia so far [8]. The structural details observed during growth and partial dissolution of the biomimetic otoconia also give rise to a first interpretation of their functionality, i.e., their response to linear accelerations. Intense future research on biomimetic as well as biogenic otoconia is needed to fully clarify the complex composite structures, their morphogenesis and their functionality.

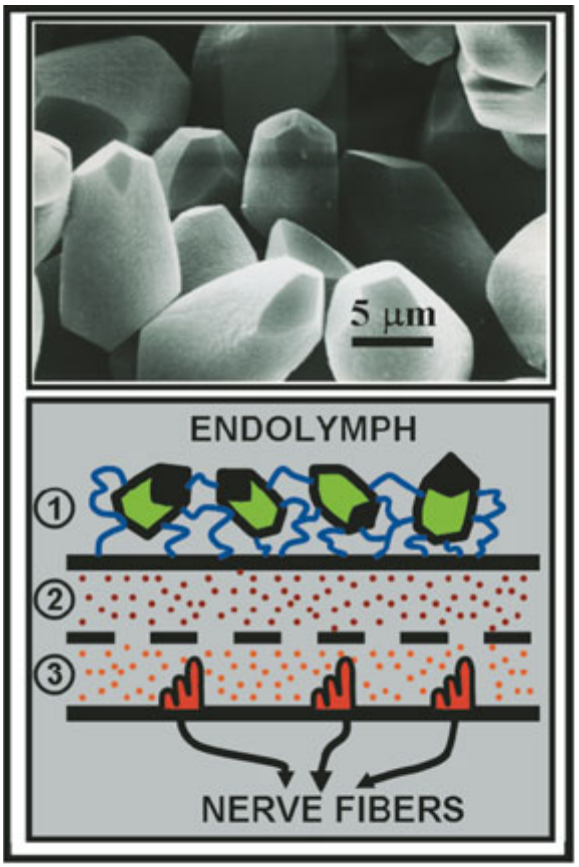

Fig. 1: Top: Calcite otoconia of guinea pig (SEM-image) showing the barrel-shaped habit with triplanar faceted ends. Bottom: Schematic sketch of the gravity receptor organ (macula) within the inner ear of mammals. ① Otoconial mass (black/green particles) in contact with endolymph and interconnected to a gelatineous matrix (② otoconial membrane) by surface adhesion and by confinement within a loose interotoconial filament matrix (blue lines in ①) [7]. ③ Sensory epithelium receiving (via hair sensors) and forwarding (via nerve fibers) information on linear accelerations. The inner ear contains two different maculae called saccular and utricular, respectively.

Characteristics of biogenic otoconia of mammals

The following features seem to be evident for otoconia of mammals although the various aspects reported up to now do not merge into a conclusive picture in general (Throughout the text we will

refer to the following assignment of the features (i.-vi.) which are comparatively discussed.):

i. The typical (adult) configuration of either saccular or utricular otoconia is a cylindrical body with terminal rhombohedral faces intersecting at the pointed ends. The symmetry of otoconia is close to $\bar{3}$ m (depending on the extension of the rhombohedral faces which may differ not only at both ends) [7,9,10].

ii. Otoconia represent composite systems consisting of ordered calcite microcrystals together with proteins (mainly glycoproteins and glycosaminoglycans) forming fibrils. They resemble the patterns of fibril packing in bone and teeth [7,11,12].

iii. No data concerning the amount of organic components in otoconia are available, yet. Therefore, a value of about 2.25 wt.-% which was reported for aragonitic plaice-otoliths [9] is used as an approximate guideline. This value is representative for biocomposites containing small amounts of organic material. It is also generally consistent with a report on rat otoconia which were described to contain only "small" amounts of organic material (proteins) [28].

iv. At least two different kinds of structure are present in otoconia: A first, more dense structure and a second, more porous one [7]. The higher material density seems to be present in direction towards the rhombohedral end-faces [10].

v. The mean size (length) of otoconia is about 10 µm [13] but even giant otoconia up to 80 µm in length are observed [14].

vi. There are some indications already that (at least parts of) otoconial specimen behave like single crystals [9,15,16].

Although not definitely confirmed so far it can be expected that otoconia which are grown during processes of biomineralisation represent inorganic/organic composites and are structured on the nanoscale. If these otoconia also give rise to scattering properties similar to that of single crystals (see feature vi.) they may represent highly mosaic-controlled nanocomposite superstructures in a similar sense as reported for biomimetic apatite-gelatine nanocomposites [17-21]. This kind of solid matter is also called a "mesocrystalline" state [22].

Morphogenesis of biomimetic otoconia

The formation of biomimetic otoconia was first observed during our work on the morphogenesis of carbonated apatite-gelatine nanocomposites by double-diffusion in gelatine gel matrices [8,23,24]. The otoconial specimens grow close to the calcium ion source; their complex morphogenesis is shown in Fig. 2. Within some days, the form development evolves from shape 1 (an arrangement characterized by six trumpet-like branches) via various intermediate states which are still dominated by six branches (2-7). The branches grow fast and develop their basal faces to the final state (8) where they meet at both ends thereby each forming three planar faces with straight common edges and rounded boundaries in direction to the belly region. The belly region grows with temporal delay and appears to be structured on a small particle scale but with a preferred (common) orientation of the sub-units.

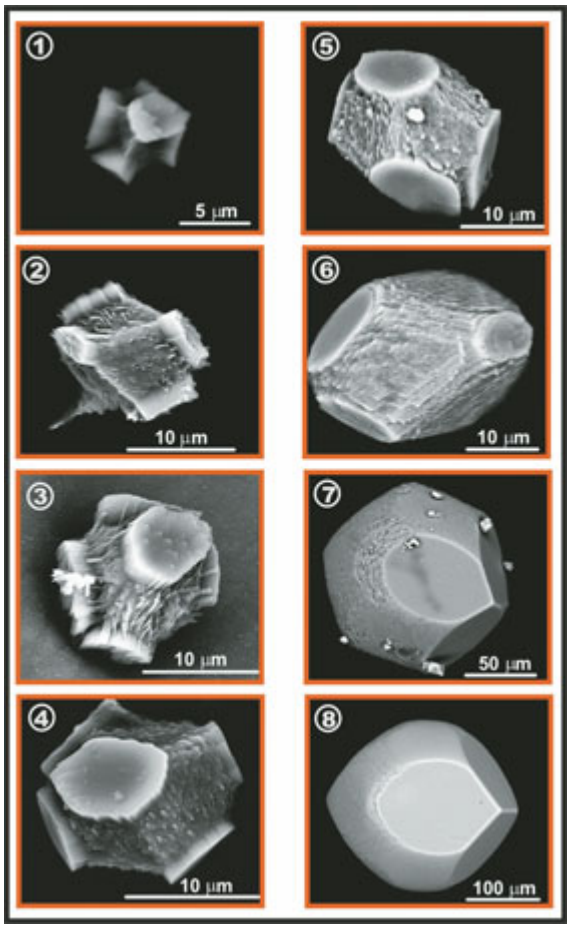

Fig. 2: Morphogenesis (sequence (1) to (8)) of biomimetic otoconia. For further details refer to the text.

Characterisation of biomimetic otoconia and comparison with biogenic species

Apart from the more pronounced and rounded belly region the biomimetic otoconia in their final state of development reveal analogous morphological characteristics as present for adult otoconia of mammals (see Fig. 1, top) with an overall symmetry close to $\bar{3}$m (see feature i.). Concerning their size the biomimetic otoconia have to be classified as "more than giant" (see feature v.). Samples investigated after a growth period of five days consist of composite particles in their final state of shape development with a size distribution between 100 µm and 400 µm. Our observations indicate already that the development of the shape to the closed otoconial habit may, in principle, be finished at a size of around 100 µm.

As summarised in Fig. 3 the biomimetic otoconia exhibit scattering properties representative for a single crystal. Even the crystal structure (calcite) could be solved by using a complete single specimen (see feature vi.) [8]. These scattering properties being so closely related to that of a single crystal are particularly remarkable by taking into account the shape development shown in Fig. 2. In fact, this development is far from classical growth processes known for single crystalline individuals. In this context it should be noted here already that the biomimetic otoconia represent an inorganic/organic composite containing an amount of gelatine between 1.9 wt.-% (Fig. 3; TG-investigations) and 2.6 wt.-% (chemical analysis), a range which is in good agreement with 2.25 wt.-% observed for aragonitic plaice otoliths (see feature iii.). The composite nature of the biomimetic otoconia is associated with a lower density (2.563 g cm^{-3}) compared with a bulk calcite crystal (2.711 g cm^{-3}); see Fig. 3. As can also be seen from Fig. 3 the planar terminal faces are indexed as "normal" rhombohedral faces (cleavage rhombohedra of calcite). A first investigation of the inner architecture of the biomimetic otoconia (SEM images) indicates the presence of two different structures: a more dense and homogeneous structure as well as a more porous one (see feature iv.).

This first SEM observation (Fig. 3) was followed up by a more detailed TEM investigation by means of a thin FIB-cut through the branch- and belly-regions of a biomimetic specimen in an early growth state (see Fig. 4). By this, it became clear

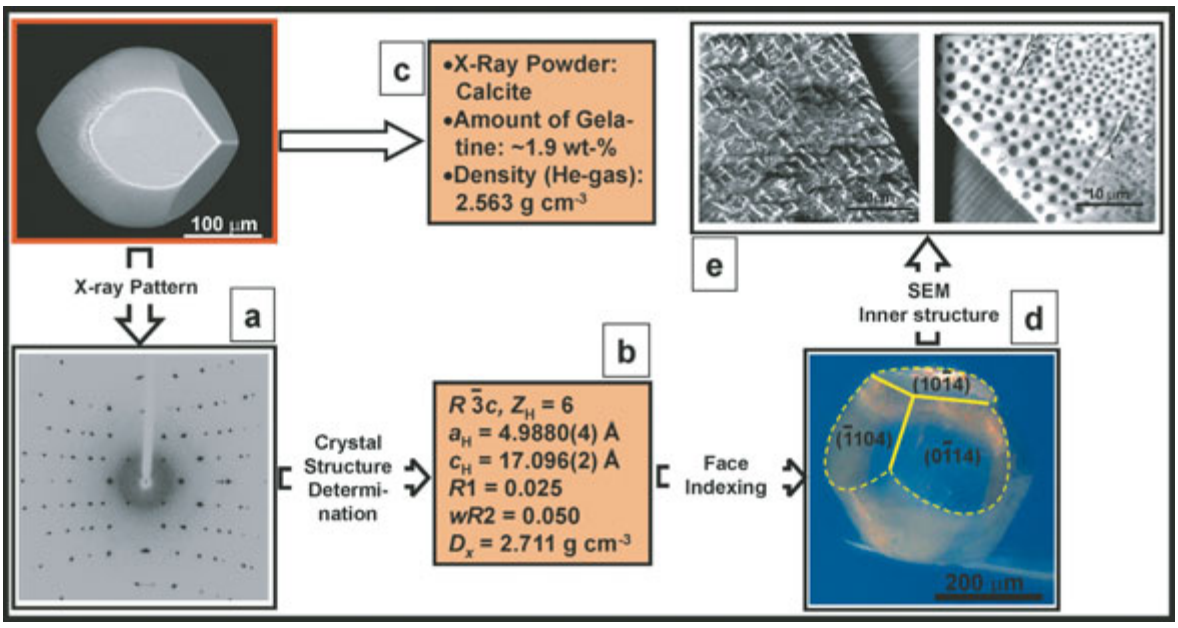

Fig. 3: Characterization of completely developed otoconial specimen (top left). Essential facts are: a) The biomimetic otoconia exhibit X-ray scattering properties which are representative for single crystals. b) The crystal structure of calcite was solved from single crystal diffraction data. c) The density of the composite (He-gas method) is significantly lower than the density of a calcite crystal. 1.9 wt.-% of gelatine contribute to the formation of the composite. d) The faces at both ends of the biomimetic otoconia were determined as "normal" rhombohedral faces (= cleavage rhombohedra of calcite). e) The inner architecture of the biomimetic otoconia is characterized (SEM-images) by two different structures: a porous structure in the belly region and a more dense structure in the branch areas.

that the branch area is characterized by a dense composite structure streaked with parallel traces of about 10 nm thickness. In analogy to our experience with apatite-gelatine-nanocomposite structures [17-21] and in accordance with the hollow tubes visible in partially decalcified otoconia (see Fig. 6) we interpret these traces as signatures of (calcified) microfibrils stretching out along the main branch direction [10$\bar{1}$4]. The high-resolution TEM image of the branch area shows a perfect periodic calcite pattern. The belly region, on the other hand, is only poorly crystalline consisting of nano-domains in a mosaic arrangement as well as of pores. The crystallographic overall-orientation of belly- and branch-areas is identical (see FFTs in Fig. 4), an observation which fully agrees with the scattering properties of the biomimetic otoconia (similar to that of a single crystal).

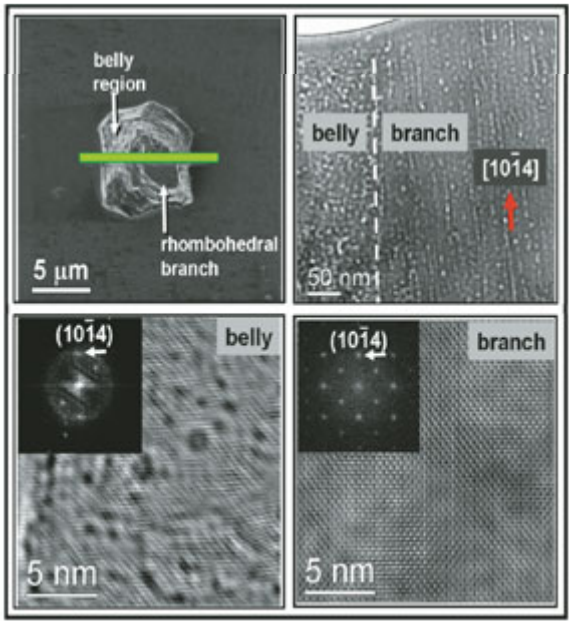

Fig. 4: Top left: Ion scanning image of a biomimetic otoconial specimen at an early stage of the morphogenesis (see Fig. 2). The green bar indicates the area from which the TEM lamella was cut by focused ion beam (FIB) technique. The cut leads through one branch oriented along the view direction. Top right: Overview TEM image of the FIB thin cut showing the structure of the composite consisting of two different areas (belly and branch). Bottom right: As evidenced by the filtered high-resolution TEM image the branch exhibits a perfect periodic pattern. Deduced from the fast Fourier transform (FFT) – inset top left – the calcite composite is viewed along [42$\bar{6}\bar{1}$]. Bottom left: The belly region is only poorly crystalline consisting of nano-domains in a mosaic arrangement as well as of pores. Compared with the branch area the FFT of the belly region (inset top left) displays only a small number of weak spots due to reduced crystallinity.

As shown in Fig. 5 the biomimetic otoconia can be decalcified by treatment with EDTA. The gelatineous residue keeps the shape of the former calcite-gelatine composite, an observation which was also made for the decalcification of rat otoconia [28]. Such kind of (partial) decalcification experiments help to obtain deeper insight into the inner architecture of the biomimetic otoconia as well as the structural correlations between the inorganic and organic components. These investigations may also provide a chance to find and isolate the central seed area which keeps the intrinsic code for this particular form development. Fig. 6 shows a SEM image of biomimetic otoconial specimen after partial decalcification. In accordance with the TEM investigations indicating a more dense structure for the branches (Fig. 4) the SEM image (Fig. 6) clearly reveals that these regions are less soluble compared with the porous and less ordered belly area. It becomes also evi-

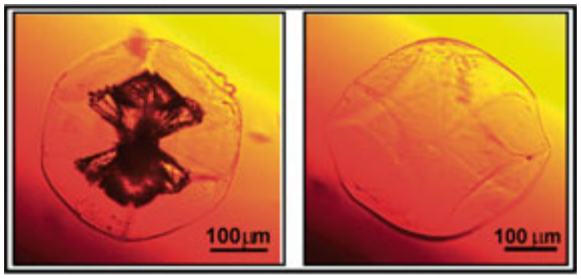

Fig. 5: Light-optical micrographs: Successive decalcification of biomimetic otoconia by EDTA (0.25 mol L^{-1}) reveals that the belly parts are easier decalcified than the branch parts confirming the different inner structure as presented in Fig. 4. Left: After treatment with EDTA for 1 h. Right: After treatment with EDTA for 2 h (The decalcified gelatine keeps its composite shape).

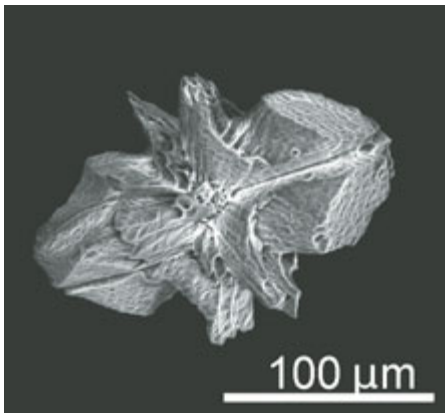

Fig. 6: SEM image of a biomimetic otoconial specimen after partial decalcification by an EDTA solution. For further details see text.

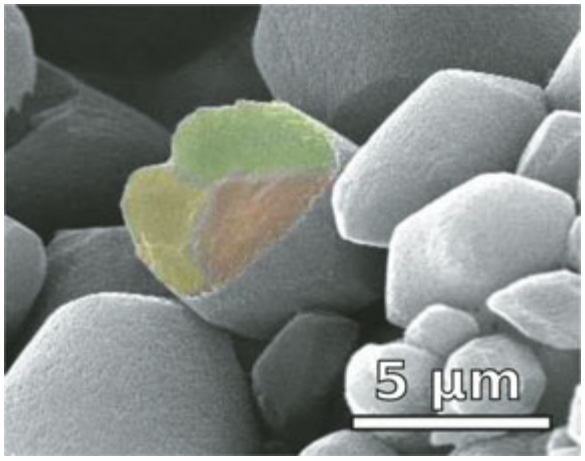

Fig. 7: SEM image of guinea pig otoconia with colored fracture area.

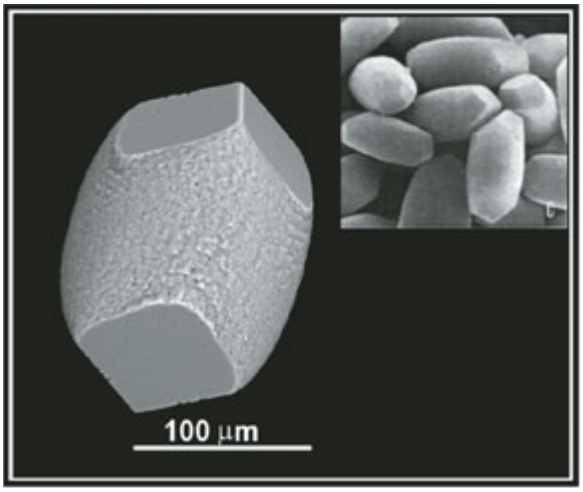

Fig. 8: "Form-correction" of biomimetic otoconia. Compared with human otoconia (inset top right) [10] the biomimetic otoconia (Fig. 2, bottom right, No. 8; Fig. 3, top left) reveal a more pronounced bulbous belly region. This region can be flattened and elongated by using a mixture of agar and gelatine as the diffusion-matrix [8]. By this, the morphology of the biomimetic otoconia (main part of this figure) is brought closer to that of human otoconia.

dent from the SEM image (Fig. 6) that the interactions between the organic and the inorganic components of the composite take place at a high level of structural order. The hollow tubes appearing on the rhombohedral faces represent the positions of the former organic fibrils extending from the center of the architecture in direction of the faces at both ends of the specimen (see also Fig. 4).

The shape development of biomimetic otoconia (Fig. 2) and their decalcification behavior (Figs. 5 and 6) clearly point at the existence of three distinct growth directions for the branch areas. The branch areas meet in the final state of shape development but do not grow perfectly into a single one: there are still significant boundary planes between their branch parts. In agreement with this characteristic feature of the biomimetic species SEM investigations of the fracture area close to the triplanar faceted ends of biogenic otoconia from guinea pig, clearly reveal the presence of three distinct regions (Fig. 7) representing the branch areas [8, 25].

On the organic components involved in the formation of otoconia

We now concentrate on the nature of the organic components involved in both, the biogenic and the biomimetic otoconia formation. Besides others [26] otoconia of mammals contain glycoproteins and glycosaminoglycans which form fibrils inside the composite structure resembling the patterns of fibril packing in bones and teeth [7, 9, 12]. Glycoproteins and glycosaminoglycans consist of macromolecules containing covalent interconnections between proteins and oligo- and polysaccharides. However, the biomimetic otoconia presented here are grown in a pure gelatine gel (denatured collagen). Following this general knowledge we simply mixed agarose with gelatine (wt.-ratio 7:3) and used the respective gel mixture as the diffusion matrix [8].

Applying this procedure the more bulbous belly region can interestingly be flattened and elongated. In result, it clearly reveals a closer relationship to the shape of otoconia of mammals as shown in Fig. 8, in comparison with human otoconia [10]. The characterization of the outer shape of otoconia (biomimetic as well as natural) is still on a descriptive level as no definite rules are known with respect to aspect ratios and other quantifying criteria. This is an interesting problem to be solved in the near future.

Recent investigations on human otoconia

No complete picture of the 3D structure and the morphogenesis of biogenic otoconia is available up to now. The shape development of the biomimetic composite seems to be a suitable model system which, for the first time, holds the chance to investigate every growth step in detail and even

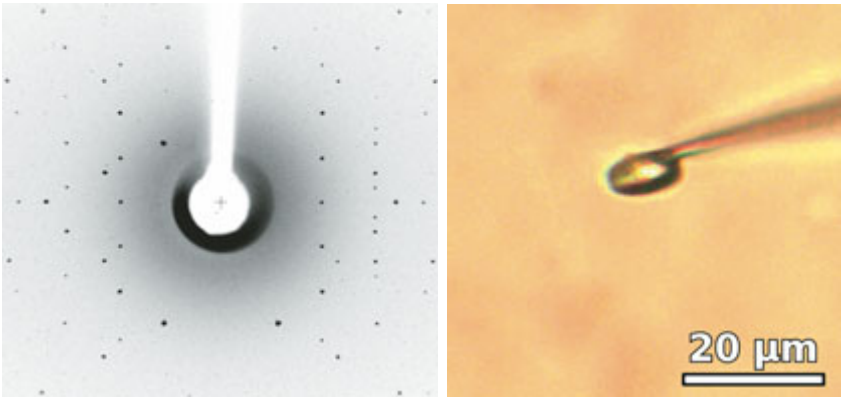

Fig. 9: X-ray diffraction pattern (left; Ag-Kα-radiation) of a single specimen (right; light-optical micrograph) of a human otoconial specimen. The crystal structure (calcite) was solved from the diffraction data ($R\bar{3}c$, Z_H=6, a_H=4.9841(8) Å, c_H=17.072(5) Å, R=0.068).

allows suitable modifications of the growth conditions. In order to check this statement in more detail, we started to investigate human otoconia by looking for further characteristic features that exceed the criteria i.-vi. given above (and which were already confirmed).

First of all, we investigated the diffraction behavior (X-ray, Ag-Kα radiation) of a complete single otoconial specimen (~ 10 µm in length). As can be seen from Fig. 9 the diffraction pattern is representative for a single crystal without indications for significant mismatch, intergrowth, or twinning. In this respect, biogenic and biomimetic (see Fig. 3) otoconia show identical diffraction characteristics.

The next essential question was focused on the decalcification behavior of human otoconia in order to find out whether the biogenic specimen are also constructed from branch- and belly-areas.

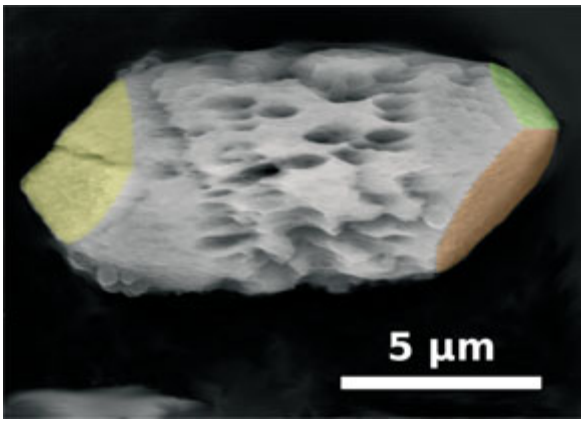

Fig. 10: SEM image of a degenerated specimen of human otoconia with colored rhombohedral faces. For further details see text.

If so, this would give a hint for the presence and distribution of different areas of structural densities. As the size of the otoconia under investigation did not exceed a value of about 10 µm we were not yet able to carry out step-by-step decalcification experiments – as performed for the biomimetic species (see Figs. 5 and 6). On the other hand, we observed a number of degenerated human otoconia revealing clear signs of decalcification processes. Such kind of degenerated human otoconial specimen is presented in Fig. 10, with the belly area being partially dissolved and streaked with larger channels. The rhombohedral branches, however, remain more or less unaffected, a picture which is consistent with the observations made on biomimetic otoconia (Figs. 5 and 6). Age-related degen-

Fig. 11: SEM image of the inside structure of an age-related degenerated human otoconial specimen [27]. For further details see text.

erated human otoconia have been subject of an early SEM investigation [27]. The images presented therein reveal similar degeneration patterns as shown in Fig. 10. Additionally, there is one image of a mechanically broken degenerated specimen (Fig. 11) [27] which could not be explained at that time but which clearly exposes its inside structure containing the three branch parts as residual stumps.

A first and careful approach towards functionality of otoconia

Although further investigations are needed for a more detailed understanding of the growth as well as the dissolution processes, a careful interpretation of the function of otoconia can already be given extending the generally accepted facts concerning weight, gravity and movement on the gelatinous matrix during linear acceleration.

Nature produces biominerals as functional materials, and their functions are reflected by their chemical constituents and by their intergrowth-structures. If the function of otoconia would be restricted to size and uniform density only (which might be suited for a response on vertical accelerations), their complex inner architecture would be insignificant. However, this is not the way nature works! The arrangement and particular distribution of areas with different (structural) densities within the otoconia are assumed to cause a peculiar mode of buoyancy within the surrounding endolymph as well as maximum displacements during translatory accelerations. The mass-distribution within otoconia leads to a mass-separation in direction of their rhombohedrally faceted ends. The center of gravity for a complete specimen is expected to be situated at (or close to) its morphological center. The otoconial mass consists of thousands of these tiny biominerals which are randomly oriented, surrounded by the endolymph (a K^+-rich electrolyte) and interconnected with the substrate (the gelatinous matrix) by surface adhesion and by confinement within a loose interotoconial filament matrix (a loose net of fibrils growing out of the otoconia and being attached to the gelatinous matrix). In case of a horizontal linear acceleration the resulting (possible) movements of an individual otoconial specimen are schematically presented in Fig. 12. During acceleration (larger green arrow pointing to the left) the inertial mass of the otoconial specimen causes a movement to the right with respect to the substrate (small green arrow) until the fibril attached at point B on the substrate is stretched (Fig. 12a to 12b). This first step of movement is followed by a rotary motion (caused by the moment of inertia) thereby turning the specimen until the fibril attached at point A on the substrate is also stretched (Fig. 12b to 12c). This highlights the fact that the peculiar inner architecture of otoconia with its dumbbell-shaped mass/density-distribution allows optimal sensing of even non-vertical translational accelerations by a combined translatory/rotary response. The transfer of force to the gelatinous matrix is then transmitted to the interconnected sensory epithelium as schematically presented in Fig. 1. As the otoconial mass within each macula consists of thousands of entities with random orientation the system is able to react to accelerations in all directions of space.

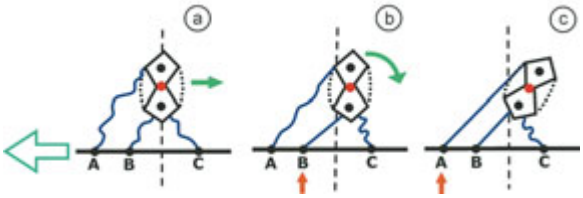

Fig. 12: Schematic sketch of the combined translatory/rotary response of an individual otoconial specimen during horizontal acceleration of a macula. Large green arrow: Direction of acceleration. Smaller green arrows: Directions of movements relative to the substrate. Blue lines: Fibrils attached to the individual otoconial specimen and to the substrate (gelatinous matrix). Red dots: Center of mass of the individual otoconia. Black dots: Illustration of the dumbbell-like mass distribution within the otoconia important for their rotational response as shown in c. For further details see text.

We would like to acknowledge fruitful cooperation and discussions with Prof. Dr. Th. Zahnert and Dr. Yuri Yarin (Klinik und Poliklinik für HNO-Heilkunde, Universitätsklinikum der TU Dresden) as well as Prof. Dr. H.-J. Hardtke and Prof. Dr. R. Schmidt (Institut für Festkörpermechanik der TU Dresden). Not least, sincere thanks to Dr. Steffen Wirth (MPI CPfS) for continuous help and participation.

References

[1] Biomineralisation: Cell Biology and Mineral Deposition *(Eds.: K. Simkiss, K. M. Wilbur),* Academic Press, San Diego (1989).

[2] Biomineralisation: Progress in Biology, Molecular Biology and Application *(Ed.: E. Bäuerlein),* Wiley-VCH, Weinheim (2004).

[3] Handbook of Biomineralization: Biological Aspects and Structure Formation *(Ed.: E. Bäuerlein),* Wiley-VCH, Weinheim (2007).

[4] *L. Addad and, St. Weiner,* Angew. Chem. **104** (1992) 159-176; Angew. Chem. Int. Ed. **31** (1992) 153-169.

[5] Biomineralisation and Biological Metal Accumulation *(Eds.: P. Westbroek, E. W. de Jong)*, D. Reidel Publ. Comp. (1983).

[6] *M. D. Ros and, K. G. Pote,* Philos. Trans. R. Soc. Lond. **B304** (1984) 445.

[7] *U. Lins, M. Farina, M. Kurc, G. Riordan, R. Thalmann, I. Thalmann, and B. Kachar,* J. Struct. Biol. **131** (2000) 67-78.

[8] *Y.-X. Huang, J. Buder, R. Cardoso-Gil, Yu. Prots, W. Carrillo-Cabrera, P. Simon, and R. Kniep,* Angew. Chem. **120** (2008) 8404-8408; Angew. Chem. Int. Ed. **47** (2008) 8280-8284.

[9] *St. Mann, S. B. Parker, M. D. Ross, A. J. Skarnulis, and R. J. P. Williams,* Proc. R. Soc. Lond. **B218** (1983) 415-424.

[10] *M. D. Ross, L.-G. Johnsson, D. Peacor, and L. F. Allard,* Ann. Otol. **85** (1976) 310-325.

[11] *H. Li and L. A. Estroff,* J. Am. Chem. Soc. **129** (2007) 5480-5483.

[12] *C. D. Fermin,* Microsc. Res. Techn. **25** (1993) 297-303.

[13] *C. G. Wright and D. G. Hubbard,* Acta Otolaryngol. **86** (1978) 185-194.

[14] *L. A. Everett, I. A. Belyantseva, K. Noben-Trauth, R. Cantos, A. Chen, S. I. Thakkar, S. L. Hoogstraten-Miller, B. Kachar, D. K. Wu, and E. D. Green,* Human. Mol. Gen. **10** (2001) 153-161.

[15] *D. Carlstrom and H. Engstrom,* Acta Otolaryngol. **45** (1955) 14-18.

[16] *D. Carlstrom,* Biol. Bull. Mar. Biol. Lab. Woods Hole **125** (1963) 441-463.

[17] *P. Simon, D. Zahn, H. Lichte, and R. Kniep,* Angew. Chem. **118** (2006) 1945-1949; Angew. Chem. Int. Ed. Engl. **45** (2006) 1911-1915.

[18] *P. Simon, W. Carrillo-Cabrera, P. Formanek, C. Göbel, D. Geiger, R. Ramlau, H. Tlatlik, J. Buder, and R. Kniep,* J. Mater. Chem. **14** (2004) 2218-2224.

[19] *P. Simon, U. Schwarz, and R. Kniep,* J. Mater. Chem. **15** (2005) 4992-4996.

[20] *H. Tlatlik, P. Simon, A. Kawska, D. Zahn, and R. Kniep,* Angew. Chem. **118** (2006) 1939-1944; Angew. Chem. Int. Ed. **45** (2006) 1905-1910.

[21] *R. Kniep, and P. Simon,* Angew. Chem. **120** (2008) 1427-1431; Angew. Chem. Int. Ed. **47** (2008) 1405-1409.

[22] *H. Cölfen, M. Antonietti,* Angew. Chem. **117** (2005) 5714-5730; Angew. Chem. Int. Ed. **44** (2005) 5576-5591. *H. Cölfen, and M. Antonietti:* Mesocrystals and Nonclassical Crystallisation, Wiley (2008).

[23] *Y.-X. Huang, R. Cardoso Gil, Yu. Prots, P. Simon, W. Carrillo-Cabrera, and J. Buder,* ECSSC XI (2007), Abstracts, W 11.

[24] *E. V. Rosseeva, J. Buder, P. Simon, U. Schwarz, O. V. Frank-Kamenetskaya, and R. Kniep,* Chem. Mater. **20** (2008) 6003-6013.

[25] *C. P. Hommerich and R. Kniep,* 57. Jahresvers. Deutsche Ges. f. Hals-Nasen-Ohren-Heilkunde, Würzburg (11.-15. Mai 1986).

[26] *Y. W. Lundberg, X. Zhao, and E. N. Yamoah,* Brain Res. **1091** (2006) 47-57.

[27] *M. D. Ross, D. Peacor, L.-G. Johnsson, andL. F. Allard,* Ann. Otol. **85** (1976) 310-326.

[28] *K. G. Pote,and M. D. Ross,* J. Ultrastruct. Res. **95** (1986) 61-70.